Environmental Science & Technology

pubs.acs.org/est

Article

Double-Edged Role of VOCs Reduction in Nitrate Formation: Insights from Observations during the China International Import Expo 2018

Yingnan Zhang, Hongli Wang,* Liubin Huang,* Liping Qiao, Min Zhou, Jiangshan Mu, Can Wu, Yujiao Zhu, Hengqing Shen, Cheng Huang, Gehui Wang, Tao Wang, Wenxing Wang, and Likun Xue*

Cite This: *Environ. Sci. Technol.* 2023, 57, 15979−15989

Read Online

ACCESS | Metrics & More | Article Recommendations | Supporting Information

ABSTRACT: Aerosol nitrate (NO_3^-) constitutes a significant component of fine particles in China. Prioritizing the control of volatile organic compounds (VOCs) is a crucial step toward achieving clean air, yet its impact on NO_3^- pollution remains inadequately understood. Here, we examined the role of VOCs in NO_3^- formation by combining comprehensive field measurements conducted during the China International Import Expo (CIIE) in Shanghai (from 10 October to 22 November 2018) and multiphase chemical modeling. Despite a decline in primary pollutants during the CIIE, NO_3^- levels increased compared to pre-CIIE and post-CIIE—NO_3^- concentrations decreased in the daytime (by −10 and −26%) while increasing in the nighttime (by 8 and 30%). Analysis of the observations and backward trajectory indicates that the diurnal variation in NO_3^- was mainly attributed to local chemistry rather than meteorological conditions. Decreasing VOCs lowered the daytime NO_3^- production by reducing the hydroxyl radical level, whereas the greater VOCs reduction at night than that in the daytime increased the nitrate radical level, thereby promoting the nocturnal NO_3^- production. These results reveal the double-edged role of VOCs in NO_3^- formation, underscoring the need for transferring large VOC-emitting enterprises from the daytime to the nighttime, which should be considered in formulating corresponding policies.

KEYWORDS: *particulate nitrate, volatile organic compounds, nitrogen oxides, oxidants, multiphase chemical box model*

INTRODUCTION

Haze pollution, characterized by high concentrations of fine particulate matter ($PM_{2.5}$), poses significant air quality issues across the globe's urban and industrialized regions.[1−3] It can impair visibility, and adversely affect climate and human health.[4,5] In response, China's central government has implemented regulations to curb $PM_{2.5}$ pollution, restricting emissions of PM, sulfur dioxide (SO_2), and nitrogen oxides (NO_x = NO + NO_2). These stringent pollutant controls have notably reduced concentrations of sulfate (SO_4^{2-}) and $PM_{2.5}$.[6−8] In contrast, the concentrations of nitrate (NO_3^-) showed an insignificant trend, and the mass fraction of NO_3^- in $PM_{2.5}$ showed an increasing trend, despite a reduction in NO_x emissions (by −26% during 2010−2020).[6−11] In cities such as Beijing, Shanghai, and Ji'nan, the contribution of NO_3^- contribution to $PM_{2.5}$ mass has surpassed that of SO_4^{2-}, becoming the primary component of secondary inorganic aerosols (SIAs).[6−8,10,11] Hence, gaining a better understanding of the NO_3^- formation regime is crucial for devising effective strategies against NO_3^- and $PM_{2.5}$ pollution.

The chemical production of NO_3^- is mainly governed by two pathways, i.e., the hydroxyl radical ($^{\bullet}OH$)-initiated oxidation of NO_2, and the hydrolysis of dinitrogen pentoxide (N_2O_5) that is produced from the reaction between NO_2 and the nitrate radical ($^{\bullet}NO_3$).[12−16] The former pathway dominates in the daytime, while the latter predominates in the nighttime.[7,17] It is evident that NO_2 and oxidants play a vital role in NO_3^- production. In addition, alkaline species [e.g., ammonia (NH_3)] also have significant impacts on NO_3^- production by affecting the gas-particle partition of NO_3^-.[18−21] Given the high-NO_x and NH_3-rich conditions in most Chinese metropolitan areas, small reductions in NO_x and NH_3 emissions may not effectively alleviate NO_3^- pollution.[10,18,19,22−24] In contrast, a high level of oxidants presents as a major cause of rapid NO_3^- and secondary organic aerosol production in megacities like Beijing, Shanghai, and Guangzhou.[6,24−28] Recently, a control strategy focusing on volatile organic compounds (VOCs) alongside NO_x reduction was implemented to reduce both $PM_{2.5}$ and ozone (O_3) levels.[29] It should be noted that VOCs have distinct roles in oxidant production in the daytime (e.g., promote $^{\bullet}OH$

Received: June 15, 2023
Revised: September 29, 2023
Accepted: September 29, 2023
Published: October 11, 2023

production) and in the nighttime (e.g., deplete $^{\bullet}NO_3$). While existing studies have primarily examined the overall effect of reductions in NO_x and VOCs on NO_3^- pollution,[30,31] few studies have explored the daytime or nighttime perspective.

Shanghai, one of the most developed megacities in China, has a dense population and thriving industry and transportation, contributing to economic growth but also leading to high energy consumption and a decline in air quality.[8,9,26,32] The China International Import Expo (CIIE) is a significant event held in Shanghai. To ensure favorable air quality during the event, strict regional-collaborative emission reduction measures were implemented in Shanghai and its surrounding areas from first to 10th in November 2018 (https://www.gov.cn/). These measures targeted reducing NO_x and VOCs emissions from various sources such as power, boiler and furnace, ultralow steel, transportation, and other industrial activities. This provides a unique opportunity to assess the impact of joint control of NO_x and VOCs on the NO_3^- production in real-world scenarios. In this study, we examine the intricate mechanisms through which the reduction of NO_x and VOCs, particularly for VOCs, influences daytime [6−17:00 local time (LT)] and nighttime (18−5:00 LT) NO_3^- production. We further discuss the nonlinear relationship between NO_x, VOCs, and NO_3^-.

MATERIALS AND METHODS

Field Observations. The field observation was conducted at an urban site (see Figure S1 for the location of the site) in Shanghai, China, from 10 October to 22 November 2018. The entire campaign was divided into three periods, i.e., pre-CIIE (10−31 October), CIIE (1−10 November), and post-CIIE (11−22 November), based on the time of the implementation and cancellation of emission control measures. Real-time measurements were taken for O_3, SO_2, NO, NO_2, VOCs, $PM_{2.5}$, water-soluble gases (HCl, HNO_2, HNO_3, and NH_3), water-soluble inorganic ions in $PM_{2.5}$ (SO_4^{2-}, NO_3^-, Cl^-, NH_4^+, Na^+, K^+, Ca^{2+}, and Mg^{2+}), particle size and number, and various meteorological parameters [temperature, relative humidity (RH), pressure, and wind direction and speed], with standard commercial techniques that followed strict quality assurance and quality control procedures.[8] Detailed information about the observational site and measurement methods is provided in the Supporting Information.

Multiphase Chemical Box Model. A multiphase chemical box model was used to investigate the effect of changes in pollutants and parameters on the detailed mechanisms for NO_3^- production. The model incorporates the regional atmospheric chemistry mechanism version 2 (RACM2) for gas-phase atmospheric chemistry and the chemical aqueous-phase radical mechanism version 2.4 (CAPRAM2.4) for aqueous-phase atmospheric chemistry.[33,34] To account for the partition of chemical species between the gas and aqueous phase, a series of gas−aqueous-phase transfer processes were established.[33] Additionally, the model incorporates physical processes such as solar radiation, diurnal evolution of the planetary boundary layer, dry deposition, and dilution with background air (see Text S2 for the parametrization of physical processes).[35−37] Three sets of simulations were conducted using the RACM-CAPRAM chemical box model, i.e., the base model simulation, sensitivity test, and empirical kinetic modeling approach (EKMA).

The base model simulation was performed to calculate the in situ NO_3^- production rates in urban Shanghai during pre-CIIE and CIIE (see Text S3 for the calculation of NO_3^- production and destruction rate). Due to the low data caption rate of VOCs (Figure S2), measurements during post-CIIE were not subjected to modeling analysis. The model was constrained by the concentrations of NO_3^-, SO_4^{2-}, Cl^-, NH_4^+, O_3, CO, NO, NO_2, SO_2, NH_3, and VOCs, as well as the temperature, RH, pressure, particle radius, liquid water content (LWC), and H^+. These inputs were averaged or interpolated into hourly resolution. Some of the aforementioned species or parameters were not measured throughout the study period, and their corresponding inputs were handled as follows. The particle radius was determined based on the measured particle number and size distribution, assuming spherical particles. The input of CO was obtained from the nearest air quality monitoring station (see its location in Figure S1). LWC and aerosol H^+ concentrations were simulated using ISORROPIA II with forward mode and metastable state (http://isorropia.eas.gatech.edu/) (Figure S3).[38,39] The performance of ISORROPIA II was validated by the good agreement between the observed and simulated NH_3 concentrations (Figure S4). The model was initiated at 00:00 LT on 10 October and ended at 23:00 LT on 10 November, with an integration step of 1 h. Prior to each simulation, the model was prerun for 1 day to approach a steady state to stabilize the concentrations of unconstrained species.

A series of sensitivity tests were performed to quantify the effect of changes in major species and parameters on NO_3^- production. These tests were conducted by rerunning the base models again for pre-CIIE while adjusting the input of NO_x, VOCs, NH_3, and LWC individually. The input of the specific pollutant or parameter was adjusted following eq 1, while other pollutants and parameters were fixed. Consequently, the differences in the in situ NO_3^- production rates between the sensitivity tests and base runs can be ascribed to changes in the target pollutant or parameter.

$$ADJ_{real\text{-}time} = PRE_{real\text{-}time} \times (IN_{AVE}/PRE_{AVE}) \quad (1)$$

where IN_{AVE} and PRE_{AVE} refer to the average diurnal profile of the target pollutant or parameter during CIIE and pre-CIIE, respectively; $PRE_{real\text{-}time}$ represents the time series of the target pollutant or parameter observed during pre-CIIE, and $ADJ_{real\text{-}time}$ represents the adjusted time series of the target pollutant or parameter.

The NO_3^- isopleth diagram (i.e., the EKMA plot) was established to aid in the development of efficient control strategies against NO_3^- pollution. We designed a 1 day model input that encompassed emission rates of NO, NO_2, VOCs, SO_2, CO, and NH_3, as well as data on the temperature, RH, pressure, particle radius, LWC, and aerosol H^+. These values were derived from measurements taken during the pre-CIIE period. Detailed information on the calculation of emission rates can be found in the Supporting Information and previous studies.[36,37,40,41] The initial chemical conditions were established by using observational data. NO_3^- and O_3 were initialized and then their formation and chemistry were simulated with inputs of other relevant species in the following integration. The model was initiated at 6:00 LT, with an integration step of 1 h and a total duration of 24 h. Prior to each simulation, the model was prerun for 1 day to approach a steady state to stabilize the concentrations of unconstrained species. A base run and a series of emission-reduction runs were performed, using X folds reductions (0−1 fold with a bin precision of 0.05) for the emission rates of NO_x and

https://doi.org/10.1021/acs.est.3c04629
Environ. Sci. Technol. 2023, 57, 15979−15989

Table 1. Summary of NO_3^-, Related Species, and Meteorological Parameters during Pre-CIIE, CIIE, and Post-CIIE in 2018[a]

species/ parameters	all					day					night				
	pre-CIIE	*p*1	CIIE	post-CIIE	*p*2	pre-CIIE	*p*1	CIIE	post-CIIE	*p*2	pre-CIIE	*p*1	CIIE	post-CIIE	*p*2
NO_3^- ($\mu g \cdot m^{-3}$)	6.4 ± 7.2	0.33	6.9 ± 6.5	6.8 ± 7.3	0.86	5.8 ± 5.7	0.26	5.2 ± 5.1	7.0 ± 7.9	<0.05	8.0 ± 8.9	<0.05	8.6 ± 7.3	6.6 ± 6.7	<0.05
SO_4^{2-} ($\mu g \cdot m^{-3}$)	4.4 ± 2.9	<0.01	3.9 ± 1.6	5.2 ± 3.0	<0.01	4.6 ± 3.0	<0.01	3.7 ± 1.5	5.4 ± 3.3	<0.01	4.3 ± 2.9	0.45	4.0 ± 1.7	4.9 ± 2.7	<0.01
NH_4^+ ($\mu g \cdot m^{-3}$)	3.3 ± 3.2	0.60	3.4 ± 2.6	4.1 ± 3.6	<0.05	3.2 ± 2.8	<0.18	2.8 ± 2.2	4.1 ± 3.9	<0.01	3.7 ± 3.8	0.09	4.0 ± 2.9	4.0 ± 3.4	0.99
Cl^- ($\mu g \cdot m^{-3}$)	0.5 ± 0.4	<0.01	0.4 ± 0.2	0.7 ± 0.5	<0.01	0.5 ± 0.4	<0.01	0.4 ± 0.2	0.7 ± 0.5	<0.01	0.6 ± 0.4	<0.01	0.4 ± 0.2	0.7 ± 0.4	<0.01
$PM_{2.5}$ ($\mu g \cdot m^{-3}$)	26.7 ± 19.3	0.36	25.5 ± 16.1	30.3 ± 24.5	<0.01	25.2 ± 17.2	<0.05	21.5 ± 13.9	30.3 ± 24.3	<0.01	30.7 ± 22.4	0.53	29.4 ± 17.2	30.3 ± 24.8	0.73
$NO_3^-/PM_{2.5}$	0.20 ± 0.09	<0.01	0.23 ± 0.10	0.20 ± 0.08	<0.01	0.20 ± 0.09	0.79	0.20 ± 0.08	0.19 ± 0.08	0.43	0.22 ± 0.10	<0.01	0.25 ± 0.11	0.21 ± 0.08	<0.01
NO_x (ppbv)	26.8 ± 13.8	<0.01	23.7 ± 11.4	28.4 ± 17.2	<0.01	26.6 ± 14.4	<0.05	23.0 ± 11.8	30.3 ± 17.7	<0.01	28.1 ± 14.1	<0.05	24.4 ± 11.0	26.5 ± 16.5	0.22
NO (ppbv)	4.9 ± 6.9	<0.01	3.6 ± 3.7	5.8 ± 9.2	<0.01	6.4 ± 8.2	<0.05	4.9 ± 4.8	6.7 ± 9.4	<0.05	3.4 ± 4.9	<0.01	2.2 ± 0.6	5.0 ± 8.9	<0.01
O_3 (ppbv)	35.6 ± 17.7	<0.01	30.8 ± 15.6	28.0 ± 12.7	0.05	40.7 ± 19.1	<0.01	32.9 ± 16.9	29.1 ± 13.3	<0.05	28.3 ± 15.8	0.13	28.8 ± 13.8	27.0 ± 12.1	0.50
VOCs (ppbv)	17.8 ± 13.4	<0.01	14.8 ± 7.9			15.4 ± 10.9	0.09	13.7 ± 8.0			20.3 ± 15.2	<0.01	15.9 ± 7.6		
NH_3 (ppbv)	6.2 ± 2.4	<0.01	4.3 ± 1.6	3.8 ± 1.8	<0.01	6.5 ± 2.5	<0.01	4.3 ± 1.7	3.9 ± 2.0	0.07	6.1 ± 2.4	<0.01	4.2 ± 1.4	3.6 ± 1.6	<0.01
SO_2 (ppbv)	1.7 ± 1.2	<0.01	0.9 ± 0.4	1.1 ± 0.6	<0.01	1.9 ± 1.4	<0.01	1.0 ± 0.4	1.2 ± 0.6	<0.01	1.5 ± 0.9	<0.01	0.9 ± 0.3	1.0 ± 0.5	0.25
temperature (°C)	18.3 ± 2.9	<0.01	16.6 ± 3.3	14.1 ± 2.5	<0.01	19.6 ± 2.8	<0.01	17.5 ± 3.2	14.8 ± 2.5	<0.01	16.8 ± 2.2	<0.01	15.6 ± 3.1	13.4 ± 2.3	<0.01
relative humidity (%)	63 ± 18	<0.01	75 ± 15	80 ± 15	<0.01	57 ± 19	<0.01	71 ± 16	77 ± 16	<0.01	71 ± 17	<0.01	79 ± 12	83 ± 13	<0.05

[a]Statistical significance tests were performed using a double-tailed Student's *t*-test, with *p*1 for comparison between CIIE and pre-CIIE and *p*2 for comparison between CIIE and post-CIIE. CIIE, China International Import Expo. Daytime: 6−17:00 LT; nighttime: 18−5:00 LT.

https://doi.org/10.1021/acs.est.3c04629
Environ. Sci. Technol. 2023, 57, 15979−15989

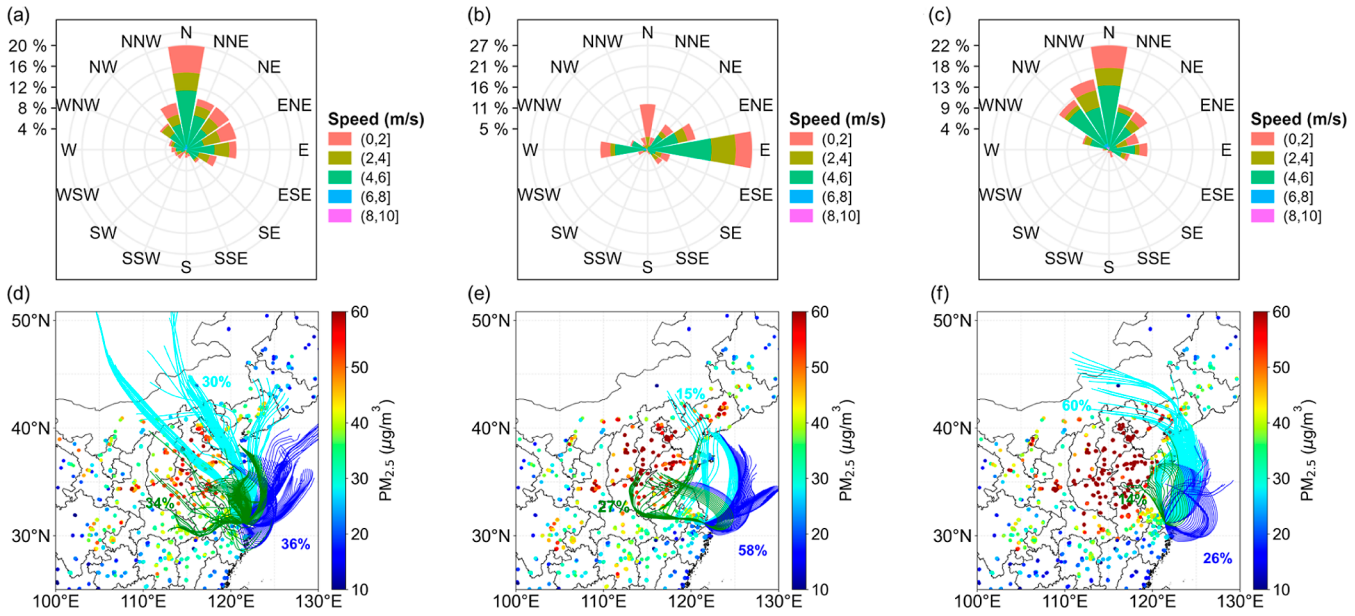

Figure 1. Wind rose plots during (a) pre-CIIE, (b) CIIE, and (c) post-CIIE. 48 h back trajectories at 1 h intervals at a height of 200 m during (d) pre-CIIE, (e) CIIE, and (f) post-CIIE. The inserted percentages represent the percentages of trajectory numbers of each classification in the whole trajectories during pre-CIIE, CIIE, and post-CIIE.

anthropogenic VOCs (AVOCs). The simulated NO_3^- concentrations were obtained for the base scenario and 399 emission reduction scenarios to illustrate the nonlinear response of NO_3^- concentrations to reductions in NO_x and AVOCs. In addition, multiple emission-reduction simulations were performed to examine the effect of different $\Delta AVOCs_{day}/\Delta AVOCs_{night}$ ratios (representing the ratio of reduction in AVOCs emission in the daytime and nighttime) on nocturnal NO_3^- concentrations.

RESULTS AND DISCUSSION

Increase in NO_3^- Concentrations during CIIE. Table 1 summarizes the average concentrations of gaseous pollutants (e.g., SO_2, NO_x, and VOCs), $PM_{2.5}$, and secondary inorganic aerosols (e.g., NO_3^-, SO_4^{2-}, and NH_4^+) during the campaign. Most pollutants exhibited a decrease in their concentration during the CIIE period. For instance, SO_4^{2-} concentration was 4.4 ± 2.9 $\mu g \cdot m^{-3}$ before the CIIE, and then this value decreased by ∼11% during CIIE. This decline can be attributed to the reduction in SO_2 concentration, from 1.7 ± 1.2 to 0.9 ± 0.4 ppbv. The average concentration of $PM_{2.5}$ during the pre-CIIE (26.7 ± 19.3 $\mu g \cdot m^{-3}$) was ∼1.1 times higher than that during the CIIE (25.5 ± 16.1 $\mu g \cdot m^{-3}$). The reduction in concentrations of gaseous and particulate pollutants during the CIIE indicates the effectiveness of the implemented stringent emission reduction measures. This finding is supported by the recovery of pollutant concentrations after CIIE (Table 1). However, the NO_3^- concentration exhibited an opposite trend, showing a slight increase during the CIIE, despite observed decreases of 12% for NO_x and 17% for VOCs. This unexpected rise in NO_3^- also led to an increased contribution of NO_3^- to the $PM_{2.5}$ mass (Table 1).

Regional transport did not appear to contribute to the elevated NO_3^- concentrations observed during CIIE. Analysis of surface winds during CIIE revealed prevailing easterly winds, with air masses mainly originating from the sea (Figures 1 and S5). The reduced frequency of air masses arriving from the south of Shanghai, an industrialized and port-intensive area, also suggested a significant decrease in the levels of pollutants contributed by transport. Local meteorological factors like temperature and RH varied noticeably during CIIE compared to pre-CIIE and post-CIIE periods (Table 1). During CIIE, relative to pre-CIIE, there was a rise in RH and a drop in temperature, leading to an increased LWC (Figure S6). This provided a greater medium for gas-particle conversion,[42] thereby facilitating NO_3^- production. Nonetheless, even with more conducive meteorological conditions in the post-CIIE period (rising RH and falling temperature), the NO_3^- levels declined (Table 1). This implies that the local chemistry triggered by changes in pollutants may play an important role in the observed NO_3^- enhancements.

During CIIE, relative to pre-CIIE and post-CIIE, NH_x (NH_3 + NH_4^+) concentrations changed by −16 and −5%, respectively (Table 1). Despite these changes in NH_x concentrations, gas ratio (GR; eq 2)[6] values consistently exceeded 1 (Figure S7), indicating a persistent NH_3-rich condition in urban Shanghai. Thus, the availability of alkaline species is not the key limiting factor for the production of NO_3^- production. We further examined the diurnal variation in NO_3^- concentration and related pollutants during CIIE. The results revealed that control measures targeting the reduction of daytime NO_x and VOCs concentrations effectively alleviated NO_3^- pollution (Figure 2). The daytime NO_3^- concentration decreased from 5.8 to 5.2 $\mu g \cdot m^{-3}$ compared to the pre-CIIE. In contrast, the reduction in nighttime NO_x and VOCs concentrations facilitated the NO_3^- production, with the nocturnal NO_3^- concentration increasing by 8% compared to pre-CIIE. The insufficient control of NO_3^- pollution during CIIE was likely due to unexpectedly higher nighttime NO_3^- production. Moreover, given that the concentrations of NO_x and VOCs declined in both daytime and nighttime (Figures 2 and S8), the different responses of NO_3^- suggest a nonlinear relationship between NO_x, VOCs, and NO_3^-.

https://doi.org/10.1021/acs.est.3c04629
Environ. Sci. Technol. 2023, 57, 15979−15989

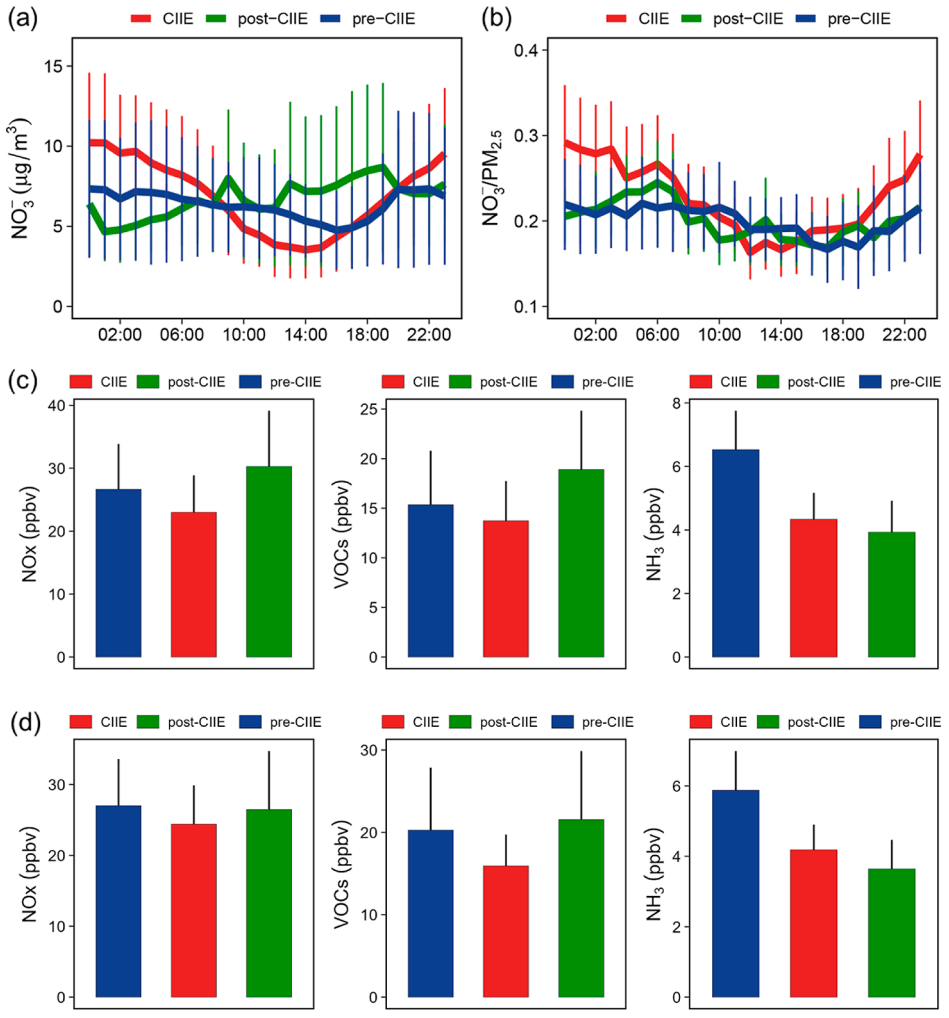

Figure 2. (a,b) Average diurnal variations in NO_3^- concentration and $NO_3^-/PM_{2.5}$ ratio in urban Shanghai during pre-CIIE, CIIE, and post-CIIE. (c) The daytime concentrations of NO_x, VOCs, and NH_3 in urban Shanghai during pre-CIIE, CIIE, and post-CIIE. (d) The nighttime concentrations of NO_x, VOCs, and NH_3 in urban Shanghai during pre-CIIE, CIIE, and post-CIIE. The error bars indicate half the standard deviation of the mean.

$$GR = \frac{([NH_3] + [NH_4^+]) - 2 \times [SO_4^{2-}]}{[NO_3^-] + [HNO_3]} \quad (2)$$

where GR refers to the gas ratio value; $[NH_3]$, $[NH_4^+]$, $[SO_4^{2-}]$, $[NO_3^-]$, and $[HNO_3]$ represent the molar concentrations of NH_3, NH_4^+, SO_4^{2-}, NO_3^-, and HNO_3, respectively.

Impact of Changes in Major Species or Parameters on NO_3^- Production. A detailed multiphase chemical box model was employed to investigate the mechanism behind the diurnal response of NO_3^- (Figure 3). The rate of NO_3^- production was calculated by the model with constraints of the observation data. In the pre-CIIE, the average NO_3^- production rate was calculated as 1.51 ± 0.57 $\mu g \cdot m^{-3} \cdot h^{-1}$ in the daytime and 0.83 ± 0.58 $\mu g \cdot m^{-3} \cdot h^{-1}$ in the nighttime (Figure 3a). During the CIIE, this value is calculated as 1.07 ± 0.49 $\mu g \cdot m^{-3} \cdot h^{-1}$ in the daytime and 1.27 ± 0.84 $\mu g \cdot m^{-3} \cdot h^{-1}$ in the nighttime (Figure 3a). The model results also showed a decrease in daytime NO_3^- production and an increase in nocturnal NO_3^- production, which is consistent with the observation. We calculated the nitrogen oxidation ratio (NOR; eq 3), finding a decrease in daytime NOR values (−10%) and an increase in the nighttime (38%), compared to pre-CIIE (Figure 3b). This suggests that increased nocturnal NO_3^- production may be linked to an increasing oxidant level. Within the defined pathways (see Text S3 for the calculation of NO_3^- production), the rates of NO_3^- production from $^{\bullet}OH + NO_2$ decreased, whereas those from N_2O_5 hydrolysis increased. Consequently, the contribution of N_2O_5 hydrolysis to NO_3^- production increased from 38% during pre-CIIE to 48% during CIIE (Figure 3c).

$$NOR = \frac{[NO_3^-]}{[NO_3^-] + [NO_x]} \quad (3)$$

where NOR refers to the nitrogen oxidation ratio; $[NO_3^-]$ and $[NO_x]$ represent the molar concentrations of NO_3^- and NO_x, respectively.

We conducted a comprehensive analysis of the individual effects of decreased levels of NO_x and VOCs on the NO_3^- production. The pre-CIIE period was selected as a baseline, and sensitivity tests were conducted by adjusting the input of NO_x or VOCs based on measurements during CIIE. Figure 3a shows that a decrease in NO_x resulted in a slight increase in NO_3^- production both in the daytime (by 3%) and in the nighttime (by 4%). The reduction in NO_x affected NO_3^- production by influencing the levels of oxidants and precursors. Under high NO_x conditions (i.e., the case in Shanghai),

https://doi.org/10.1021/acs.est.3c04629
Environ. Sci. Technol. 2023, 57, 15979−15989

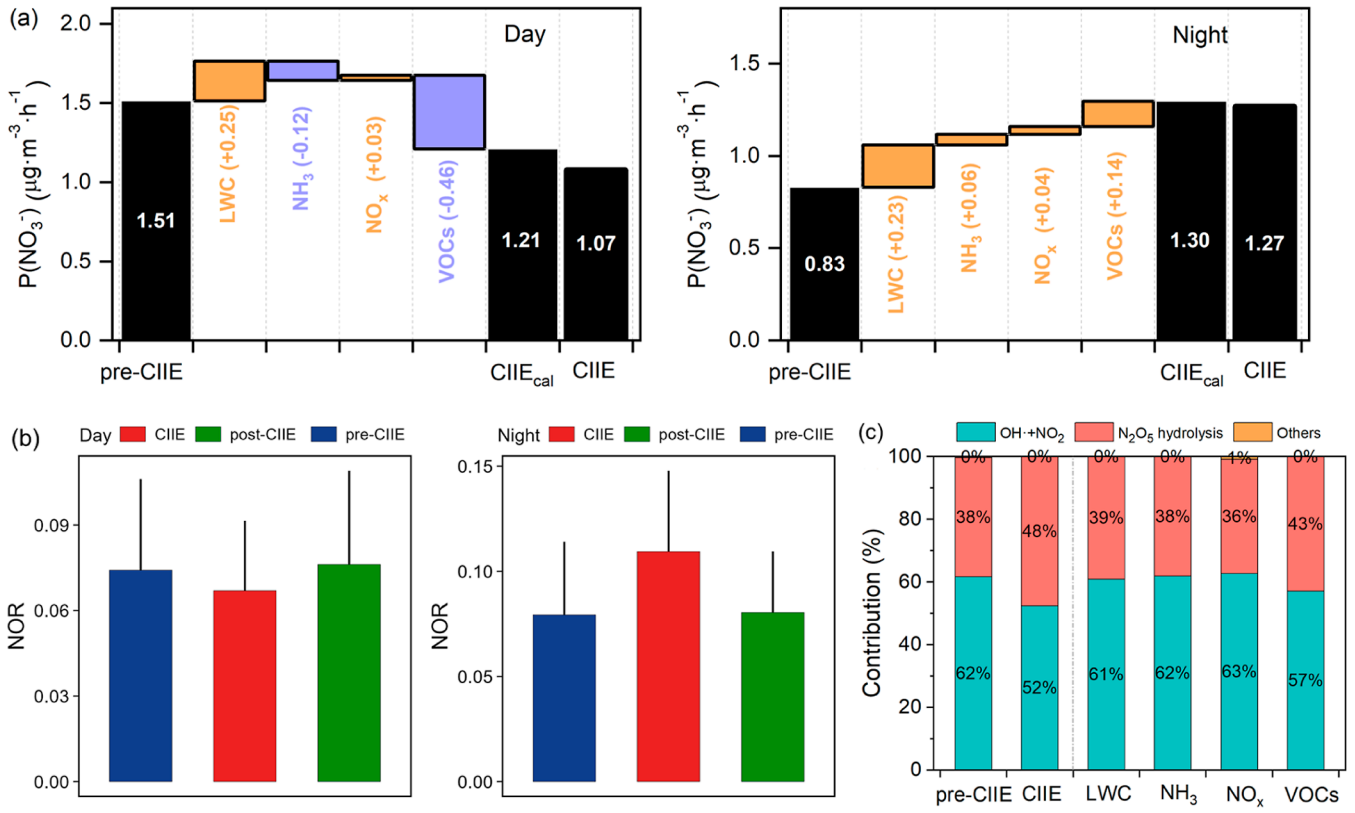

Figure 3. (a) Effect of changes in major species and parameters [e.g., NO_x, VOCs, NH_3, and liquid water content (LWC)] on the NO_3^- production. The values for pre-CIIE and CIIE were derived from base simulations, and those for $CIIE_{cal}$ were calculated as the sum of the values for pre-CIIE and the total change caused by individual species or parameters. Bars in orange represent an increase, while in purple represent a decrease. (b) Comparison of NOR in urban Shanghai during pre-CIIE, CIIE, and post-CIIE. The error bars indicate half the standard deviation of the mean. (c) The model-calculated contributions of different pathways (including $^{\bullet}OH + NO_2$, N_2O_5 hydrolysis, and other pathways) to in situ NO_3^- production under base scenarios during pre-CIIE and CIIE periods and under sensitivity tests with adjusted LWC, NH_3, NO_x, and VOCs, respectively. Refer to Text S3 for the NO_3^- production pathways.

decreased NO_x reduced the precursor levels and increased $^{\bullet}OH$ concentrations in the daytime, and it lowered the precursor levels and increased $^{\bullet}NO_3$ concentrations at night (Figures 4 and S9). The opposing effects of NO_x reduction on oxidants and precursors could offset each other, resulting in a minor promotional effect on N_2O_5 (refer to Figure 4f and the $^{\bullet}NO_3 + NO_2$ pathway in Figure S9A) and NO_3^- production. Intriguingly, the decrease in VOCs resulted in quite different impacts on daytime and nighttime NO_3^- production. Decreased VOCs significantly reduced daytime NO_3^- production (by −31%), but prompted nocturnal NO_3^- production (by 17%). These findings indicate that decreased VOCs strongly influence the diurnal response of NO_3^-. To explore other factors contributing to the NO_3^- response, we conducted sensitivity simulations by adjusting the input of NH_3 and LWC (Figure 3a). Changes in NH_3 had a negligible effect on the NO_3^- production. Increased LWC largely enhanced NO_3^- production, both in the daytime and at night, by providing more medium for gas-particle conversion (e.g., enhancing N_2O_5 hydrolysis), but was not associated with the diurnal NO_3^- response. Overall, the diurnal NO_3^- response primarily resulted from the double-edged role of VOCs in the NO_3^- formation.

Unlike NO_x, decreased VOCs affect NO_3^- production primarily by influencing the levels of oxidants. The double-edged role of VOCs in NO_3^- formation is attributed to their distinct roles in daytime and nighttime oxidants production. In the daytime, decreased VOCs reduce the concentrations of $^{\bullet}OH$, leading to a decrease in NO_3^- production; in comparison, at night, decreased VOCs increase the concentrations of $^{\bullet}NO_3$, thereby promoting NO_3^- production (Figure 4). During CIIE, the larger decreases in VOCs at night (−4.4 ppbv) outweighed the cumulative effect of decreases in VOCs in the daytime (−1.7 ppbv), resulting in increased nocturnal $^{\bullet}NO_3$ concentrations (Figure 4). Note that decreased VOCs decreased the rates of both $^{\bullet}NO_3$ production and $^{\bullet}NO_3$ loss pathways (except for $^{\bullet}NO_3 + NO_2$), but the impact on $^{\bullet}NO_3$ loss was larger than that on $^{\bullet}NO_3$ production, leading to an increase in $^{\bullet}NO_3$ concentrations overall. This further enhanced N_2O_5 production by accelerating the rates of $^{\bullet}NO_3 + NO_2$ (Figure S9B). Among the major VOC groups, alkenes exhibited the largest nighttime decreases (Table S1 and Figure S8) and had the largest promotional effect on nocturnal oxidants and NO_3^- production (Figure S10). Consistent with previous studies, we found an overall decreasing effect of reduced VOCs on NO_3^- production (−0.32 $\mu g \cdot m^{-3} \cdot h^{-1}$).[6,22,24] We provide additional insights into the diurnal perspective of the impact of reduced VOCs on the NO_3^- production. The results highlight that a greater reduction in VOCs at night, compared to the daytime, could increase the $^{\bullet}NO_3$ level and exacerbate nocturnal NO_3^- pollution.

Optimal Control Strategy for NO_3^- Pollution. The observation and model results indicate that larger decreases in VOCs at night, compared to those in the daytime, resulted in

https://doi.org/10.1021/acs.est.3c04629
Environ. Sci. Technol. 2023, 57, 15979−15989

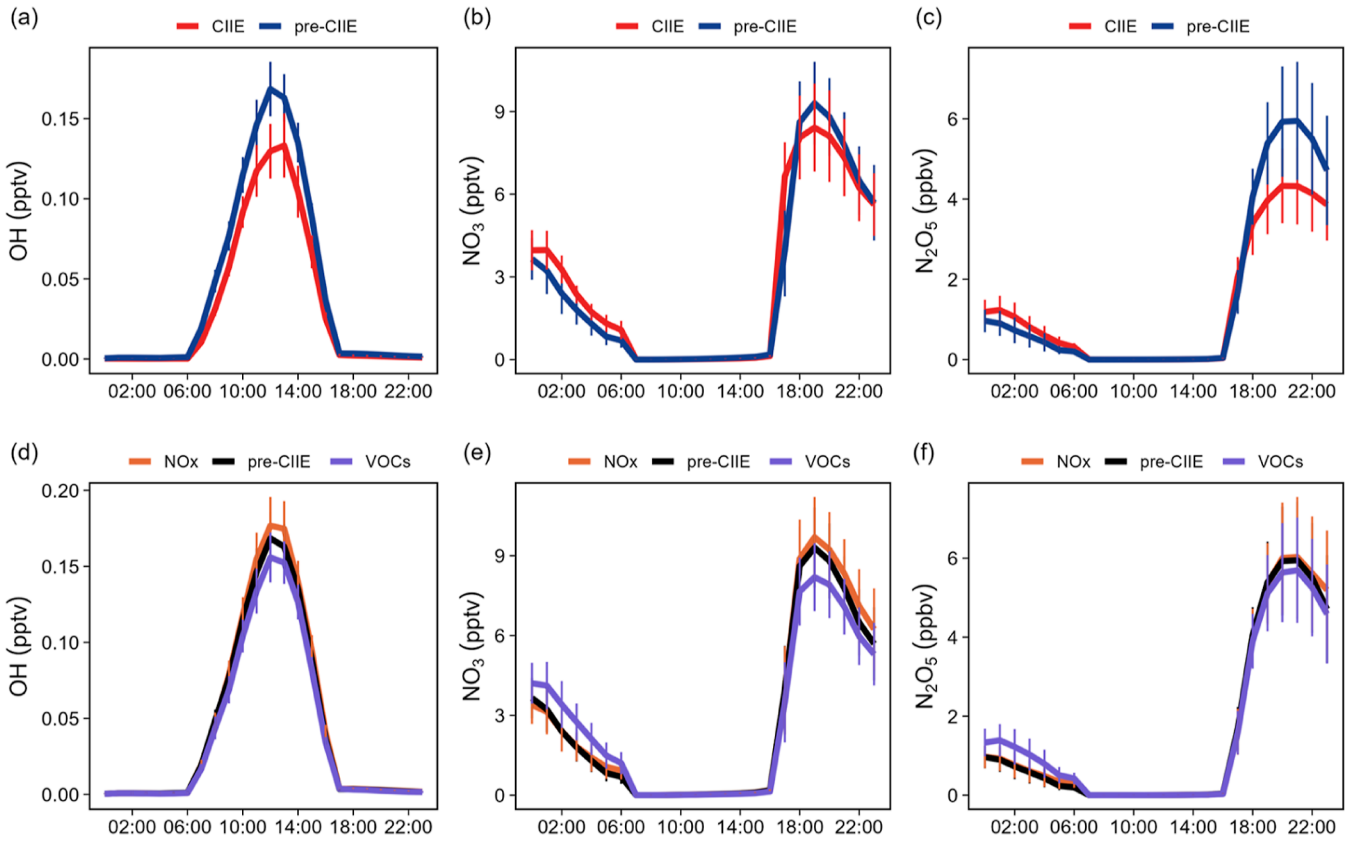

Figure 4. (a−c) Average diurnal variations in model-simulated $^{\bullet}OH$, $^{\bullet}NO_3$, and N_2O_5 concentrations during pre-CIIE and CIIE. (d−f) Comparison of $^{\bullet}OH$, $^{\bullet}NO_3$, and N_2O_5 concentrations between base scenarios and sensitivity tests. "pre-CIIE" refers to results obtained from base scenarios, while "NO_x" and "VOCs" refer to results obtained from sensitivity tests targeted at NO_x and VOCs, respectively.

higher levels of oxidants and unexpectedly higher concentrations of NO_3^- in the nighttime. To aid in the development of effective control strategies, we conducted a series of emission-reduction runs to establish the nonlinear relationships between NO_3^-, NO_x, and AVOCs. The emissions of biogenic VOCs (BVOCs) were kept fixed in the base runs and emission-reduction runs since they are beyond control efforts. The model-simulated average CO, NO_x, VOCs, O_3, and NO_3^- concentrations were 416 ppbv, 36.6 ppbv, 19.2 ppbv, 27 ppbv, and 6.3 $\mu g \cdot m^{-3}$, respectively. These values were comparable to the observations in urban Shanghai (CO: 391 ppbv; NO_x: 26.8 ppbv; VOCs: 17.8 ppbv; O_3: 35.6 ppbv; and NO_3^-: 6.4 $\mu g \cdot m^{-3}$). The good agreement demonstrates the model's capability to reproduce the observations, indicating an accurate representation of the emissions, chemistry, and physical processes.

We first examined the effect of reduction in AVOCs emissions on nocturnal NO_3^- concentrations, considering different ratios of AVOCs reduction between daytime ($\Delta AVOCs_{day}$) and nighttime ($\Delta AVOCs_{night}$). The model-simulated average AVOC concentrations were 14.5 ppbv in the daytime and 25.3 ppbv in the nighttime. As shown in Figure 5a, a reduction in AVOCs emissions could increase nocturnal NO_3^- concentrations, especially when AVOCs reduction occurs exclusively during the nighttime. The negative effect from VOC reductions on NO_3^- production disappeared when the promotional effect of nocturnal VOC reductions on NO_3^- production was negated by the cumulative effect of daytime VOC reductions, e.g., with an $\Delta AVOCs_{day}/\Delta AVOCs_{night}$ ratio of 1:1. With similar reduction scales, daytime AVOCs reduction consistently outperformed nighttime AVOCs reduction in reducing nocturnal NO_3^- concentrations. Therefore, enterprises with substantial VOC emissions should consider shifting their activities from daytime to nighttime, e.g., peak-shifts of oil uploading in the nighttime. Among the AVOC groups, aromatics had the greatest influence on reducing nocturnal NO_3^- production (Figure 5b). Nevertheless, it is challenging to reduce the 24 h average NO_3^- concentration to 3.0 $\mu g \cdot m^{-3}$ (assuming $NO_3^-/PM_{2.5}$ = 0.20 according to Table 1), which is the recommended guideline by the World Health Organization (WHO) for 24 h $PM_{2.5}$ concentration of 15 $\mu g \cdot m^{-3}$,[43] solely through AVOCs reduction. Even with 100% AVOCs reduction in the daytime, the 24 h average NO_3^- concentration could only be reduced to 3.5 $\mu g \cdot m^{-3}$, due to the influence of BVOCs and background oxidants.

In order to achieve the WHO guideline for $PM_{2.5}$ concentration, a drastic cut in NO_x emissions is required, considering the limited potential of AVOCs reduction. The control measures aim to eliminate the NO titration effect and to shift the NO_3^- formation regime from being VOC-limited to mixed-limited, and eventually to NO_x-limited conditions (refer to Figure 5). To reach the mixed-limited regime, the NO_x emission in urban Shanghai would have to be reduced by 28−70% from the levels observed during the pre-CIIE period (see the black dashed line in Figure 5), and 93% NO_x reductions would be needed to meet the WHO guideline (see the white dashed line in Figure 5c). Achieving such significant reductions in NO_x emissions necessitates transformative changes in the current energy and transportation

https://doi.org/10.1021/acs.est.3c04629
Environ. Sci. Technol. 2023, 57, 15979−15989

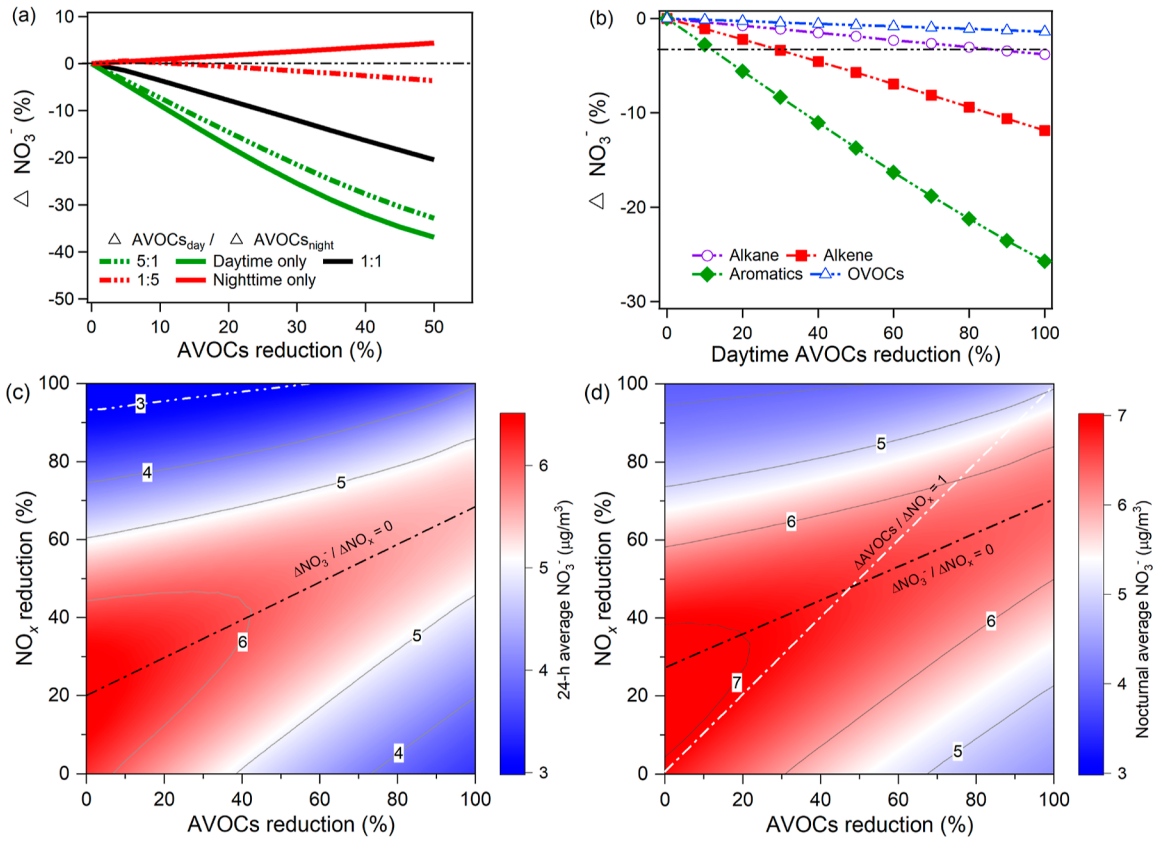

Figure 5. (a) The model-simulated change in nocturnal average NO_3^- concentrations as a function of reduction in AVOCs emission, with $\Delta AVOCs_{day}/\Delta AVOCs_{night}$ being 5:1, 1:1, and 1:5, respectively, or AVOCs reduction only occurring in the daytime or nighttime. $\Delta AVOCs_{day}/\Delta AVOCs_{night}$ represents the ratio of AVOCs reduction in the daytime and nighttime. (b) The model-simulated change in nocturnal average NO_3^- concentration as a function of reduction in alkanes, alkenes, aromatics, and OVOCs emissions in the daytime. (c) Contour plots of the simulated 24 h average NO_3^- concentration as a function of reduction in NO_x and AVOCs emission ($\Delta AVOCs_{day}/\Delta AVOCs_{night}$ = 1; $\Delta NO_{xday}/\Delta NO_{xnight}$ = 1). The black dashed line represents the boundary between the VOC-limited and mixed-limited ($\Delta NO_3^-/\Delta NO_x = 0$) NO_3^- formation regime. (d) Contour plots of the simulated nocturnal average NO_3^- concentration as a function of reduction in NO_x and AVOCs emission ($\Delta AVOCs_{day}/\Delta AVOCs_{night}$ = 1; $\Delta NO_{xday}/\Delta NO_{xnight}$ = 1). The black dashed line represents the boundary between the VOC-limited and mixed-limited ($\Delta NO_3^-/\Delta NO_x = 0$) NO_3^- formation regime. The white dashed line represents the fitting line for a base case with an $\Delta AVOCs/\Delta NO_x$ reduction ratio = 1.0 [=percentage change in emission (mol/cm^3)/percentage change in concentration (mol/cm^3)], which exerts nearly zero effect on nocturnal NO_3^- production.

sectors such as the widespread adoption of renewable energy and green transportation.

In the short term, for urban Shanghai, a combined strategy targeting AVOCs and NO_x control can be implemented to reduce nocturnal NO_3^- concentrations and simultaneously shift the NO_3^- formation regime. This strategy should prioritize a reduction ratio of $\Delta AVOCs/\Delta NO_x$ greater than 1.0 (see the white dashed line in Figure 5d), when $\Delta AVOCs_{day}/\Delta AVOCs_{night}$ = 1:1 and $\Delta NO_{xday}/\Delta NO_{xnight}$ = 1:1.

The above results are derived from the detailed measurements at one urban site in Shanghai. Similar studies in other areas would be needed in order to reveal the mechanisms by which NO_x and VOC reductions affect NO_3^- formation under different atmospheric conditions. Nonetheless, the comprehensive measurements in urban Shanghai and the model analysis provide valuable insights into the control of NO_3^- pollution in regions with meteorology and emission characteristics like Shanghai.

Atmospheric Implications. The experience of Shanghai during the CIIE provides an insightful real-world scenario for examining the response of NO_3^- pollution to the joint control of NO_x and VOCs. By combining measurements and detailed multiphase chemical modeling, we delineate the complex role of VOCs in oxidants and NO_3^- formation. In its 14th Five-Year Plan for 2021−2025, China has marked VOCs management as a major target, along with reducing NO_x emissions. It is crucial to consider the double-edged role of VOCs in the formation of secondary aerosols and oxidants when formulating corresponding policies, particularly in light of the increasing nighttime oxidation capacity and NO_3^- formation in China.[44] For cities like Shanghai, where oxidants and NO_3^- formation are under NO_x-saturated conditions, controlling AVOCs can effectively reduce oxidant and NO_3^- levels in the short term, provided that greater AVOCs reduction takes place in the daytime compared to the nighttime. This necessitates the transfer of enterprises with high VOCs emissions from daytime to nighttime, e.g., peak-shift of oil uploading in the nighttime. Our findings also indicate a limited potential for AVOCs reduction to decrease NO_3^- concentrations due to the influence of BVOCs and background oxidants. Thus, in the long run, a drastic cut in NO_x emissions is imperative, requiring transformative shifts in current energy and transportation sectors, such as rapid and large-scale adoption of renewable energy and environmentally friendly transportation.

https://doi.org/10.1021/acs.est.3c04629
Environ. Sci. Technol. 2023, 57, 15979−15989

■ ASSOCIATED CONTENT

Supporting Information

The Supporting Information is available free of charge at https://pubs.acs.org/doi/10.1021/acs.est.3c04629.

Description of observational site and measurement techniques; parametrization of physical processes within the RACM-CAPRAM model; calculation of NO_3^- production and destruction rate within the RACM-CAPRAM model; calculation of emission rate for major pollutants; comparison of VOC concentrations between pre-CIIE and CIIE; description of the location of the Yangtze River Delta, Shanghai city and the sampling site; time series of major species and meteorological parameters during the whole observational period; median diurnal profile of aerosol H^+ concentrations and LWC; comparison between observed and ISOROPIA II-simulated NH_3 concentrations; comparison of wind rose plots and 48 h backward trajectories during pre-CIIE, CIIE, and post-CIIE; comparison of LWC under base scenarios and sensitivity tests; distribution of the gas ratio; results of average diurnal variations in alkanes, alkenes, and aromatics; $^{\bullet}NO_3$ budget under base scenarios and sensitivity tests; average diurnal variations in model-simulated $^{\bullet}OH$ and $^{\bullet}NO_3$ concentrations under base scenarios and sensitivity tests (PDF)

■ AUTHOR INFORMATION

Corresponding Authors

Hongli Wang − *State Environmental Protection Key Laboratory of the Cause and Prevention of Urban Air Pollution Complex, Shanghai Academy of Environmental Sciences, 200233 Shanghai, China;* orcid.org/0000-0003-0655-3389; Email: wanghl@saes.sh.cn

Liubin Huang − *Environment Research Institute, Shandong University, 250100 Ji'nan, China*; Email: hliubin@sdu.edu.cn

Likun Xue − *Environment Research Institute, Shandong University, 250100 Ji'nan, China;* orcid.org/0000-0001-7329-2110; Email: xuelikun@sdu.edu.cn

Authors

Yingnan Zhang − *Environment Research Institute, Shandong University, 250100 Ji'nan, China; State Environmental Protection Key Laboratory of the Cause and Prevention of Urban Air Pollution Complex, Shanghai Academy of Environmental Sciences, 200233 Shanghai, China*

Liping Qiao − *State Environmental Protection Key Laboratory of the Cause and Prevention of Urban Air Pollution Complex, Shanghai Academy of Environmental Sciences, 200233 Shanghai, China*

Min Zhou − *State Environmental Protection Key Laboratory of the Cause and Prevention of Urban Air Pollution Complex, Shanghai Academy of Environmental Sciences, 200233 Shanghai, China*

Jiangshan Mu − *Environment Research Institute, Shandong University, 250100 Ji'nan, China*

Can Wu − *Key Lab of Geographic Information Science of the Ministry of Education, School of Geographic Sciences, East China Normal University, 200241 Shanghai, China;* orcid.org/0000-0003-2025-2646

Yujiao Zhu − *Environment Research Institute, Shandong University, 250100 Ji'nan, China; State Environmental Protection Key Laboratory of the Cause and Prevention of Urban Air Pollution Complex, Shanghai Academy of Environmental Sciences, 200233 Shanghai, China*

Hengqing Shen − *Environment Research Institute, Shandong University, 250100 Ji'nan, China*

Cheng Huang − *State Environmental Protection Key Laboratory of the Cause and Prevention of Urban Air Pollution Complex, Shanghai Academy of Environmental Sciences, 200233 Shanghai, China;* orcid.org/0000-0001-9518-3628

Gehui Wang − *Key Lab of Geographic Information Science of the Ministry of Education, School of Geographic Sciences, East China Normal University, 200241 Shanghai, China;* orcid.org/0000-0002-0181-4685

Tao Wang − *Department of Civil and Environmental Engineering, The Hong Kong Polytechnic University, 999077 Hong Kong, China;* orcid.org/0000-0002-4765-9377

Wenxing Wang − *Environment Research Institute, Shandong University, 250100 Ji'nan, China*

Complete contact information is available at: https://pubs.acs.org/10.1021/acs.est.3c04629

Notes

The authors declare no competing financial interest.

■ ACKNOWLEDGMENTS

We thank Dr. Xiaorui Chen from The Hong Kong Polytechnic University for the discussion about the interpretation of the results. We thank the Regional Atmospheric Chemistry Mechanism and Chemical Aqueous-Phase RAdical Mechanism development groups for the provision of the mechanisms. We also thank Tsinghua University for providing the MEIC emission inventory, and Peking University for providing a biogenic emission inventory. This work was funded by the National Natural Science Foundation of China (42075094, 42061134008, and 41922051), the National Key Research and Development Program of China (2022YFC3701101), Science and Technology Commission of the Shanghai Municipality (20dz1204002), and State Environmental Protection Key Laboratory of Formation and Prevention of Urban Air Pollution Complex (CX2020080580).

■ REFERENCES

(1) Huang, R.; Zhang, Y.; Bozzetti, C.; Ho, K.; Cao, J.; Han, Y.; Daellenbach, K.; Slowik, J.; Platt, S.; Canonaco, F.; Zotter, P.; Wolf, R.; Pieber, S.; Bruns, E.; Crippa, M.; Ciarelli, G.; Piazzalunga, A.; Schwikowski, M.; Abbaszade, G.; Schnelle-Kreis, J.; Zimmermann, R.; An, Z.; Szidat, S.; Baltensperger, U.; Haddad, I.; Prévôt, A. S. H. High secondary aerosol contribution to particulate pollution during haze events in China. *Nature* **2014**, *514* (7521), 218−222.

(2) von Schneidemesser, E.; Monks, P.; Allan, J.; Bruhwiler, L.; Forster, P.; Fowler, D.; Lauer, A.; Morgan, W.; Paasonen, P.; Righi, M.; Sindelarova, K.; Sutton, M. Chemistry and the linkages between air quality and climate change. *Chem. Rev.* **2015**, *115* (10), 3856−3897.

(3) Seinfeld, J. Urban air pollution: state of the science. *Science* **1989**, *243* (4892), 745−752.

(4) Lelieveld, J.; Evans, J.; Fnais, M.; Giannadaki, D.; Pozzer, A. The contribution of outdoor air pollution sources to premature mortality on a global scale. *Nature* **2015**, *525* (7569), 367−371.

(5) Wang, Y.; Zhang, R.; Saravanan, R. Asian pollution climatically modulates mid-latitude cyclones following hierarchical modelling and observational analysis. *Nat. Commun.* **2014**, *5* (1), 3098.

(6) Fu, X.; Wang, T.; Gao, J.; Wang, P.; Liu, Y.; Wang, S.; Zhao, B.; Xue, L. Persistent heavy winter nitrate pollution driven by increased photochemical oxidants in Northern China. *Environ. Sci. Technol.* **2020**, *54* (7), 3881−3889.
(7) Wen, L.; Xue, L.; Wang, X.; Xu, C.; Chen, T.; Yang, L.; Wang, T.; Zhang, Q.; Wang, W. Summertime fine particulate nitrate pollution in the North China Plain: increasing trends, formation mechanisms and implications for control policy. *Atmos. Chem. Phys.* **2018**, *18* (15), 11261−11275.
(8) Zhou, M.; Nie, W.; Qiao, L.; Huang, D.; Zhu, S.; Lou, S.; Wang, H.; Wang, Q.; Tao, S.; Sun, P.; Liu, Y.; Xu, Z.; An, J.; Yan, R.; Su, H.; Huang, C.; Ding, A.; Chen, C. Elevated formation of particulate nitrate from N_2O_5 hydrolysis in the Yangtze River Delta region from 2011 to 2019. *Geophys. Res. Lett.* **2022**, *49* (9), No. e2021GL097393.
(9) Wang, T.; Xue, L.; Feng, Z.; Dai, J.; Zhang, Y.; Tan, Y. Ground-level ozone pollution in China: a synthesis of recent findings on influencing factors and impacts. *Environ. Res. Lett.* **2022**, *17* (6), 063003.
(10) Xie, X.; Hu, J.; Qin, M.; Guo, S.; Hu, M.; Wang, H.; Lou, S.; Li, J.; Sun, J.; Li, X.; Sheng, L.; Zhu, J.; Chen, G.; Yin, J.; Fu, W.; Huang, C.; Zhang, Y. Modeling particulate nitrate in China: Current findings and future directions. *Environ. Int.* **2022**, *166*, 107369.
(11) Zong, Z.; Tian, C.; Sun, Z.; Tan, Y.; Shi, Y.; Liu, X.; Li, J.; Fang, Y.; Chen, Y.; Ma, Y.; Gao, H.; Zhang, G.; Wang, T. Long-term evolution of particulate nitrate pollution in North China: isotopic evidence from 10 offshore cruises in the Bohai Sea from 2014 to 2019. *J. Geophys. Res.: Atmos.* **2022**, *127* (11), No. e2022JD036567.
(12) Alexander, B.; Sherwen, T.; Holmes, C.; Fisher, J.; Chen, Q.; Evans, M.; Kasibhatla, P. Global inorganic nitrate production mechanisms: comparison of a global model with nitrate isotope observations. *Atmos. Chem. Phys.* **2020**, *20* (6), 3859−3877.
(13) Chen, X.; Wang, H.; Lu, K.; Li, C.; Zhai, T.; Tan, Z.; Ma, X.; Yang, X.; Liu, Y.; Chen, S.; Dong, H.; Li, X.; Wu, Z.; Hu, M.; Zeng, L.; Zhang, Y. Field determination of nitrate formation pathway in winter Beijing. *Environ. Sci. Technol.* **2020**, *54* (15), 9243−9253.
(14) Wang, H.; Lu, K.; Chen, X.; Zhu, Q.; Chen, Q.; Guo, S.; Jiang, M.; Li, X.; Shang, D.; Tan, Z.; Wu, Y.; Wu, Z.; Zou, Q.; Zheng, Y.; Zeng, L.; Zhu, T.; Hu, M.; Zhang, Y. High N_2O_5 concentrations observed in urban Beijing: implications of a large nitrate formation pathway. *Environ. Sci. Technol. Lett.* **2017**, *4* (10), 416−420.
(15) Wu, C.; Liu, L.; Wang, G.; Zhang, S.; Li, G.; Lv, S.; Li, J.; Wang, F.; Meng, J.; Zeng, Y. Important contribution of N_2O_5 hydrolysis to the daytime nitrate in Xi'an, China during haze periods: isotopic analysis and WRF-Chem model simulation. *Environ. Pollut.* **2021**, *288*, 117712.
(16) Yun, H.; Wang, T.; Wang, W.; Tham, Y. J.; Li, Q.; Wang, Z.; Poon, S. Nighttime NO_x loss and $ClNO_2$ formation in the residual layer of a polluted region: insights from field measurements and an iterative box model. *Sci. Total Environ.* **2018**, *622*−*623*, 727−734.
(17) Zhang, Y.; Zhang, W.; Fan, M.; Li, J.; Fang, H.; Cao, F.; Lin, Y.; Wilkins, B.; Liu, X.; Bao, M.; Hong, Y.; Michalski, G. A diurnal story of $\Delta^{17}O(NO_3^-)$ in urban Nanjing and its implication for nitrate aerosol formation. *npj Clim. Atmos. Sci.* **2022**, *5* (1), 50.
(18) Fu, X.; Wang, S.; Xing, J.; Zhang, X.; Wang, T.; Hao, J. Increasing ammonia concentrations reduce the effectiveness of particle pollution control achieved via SO_2 and NO_x emissions reduction in East China. *Environ. Sci. Technol. Lett.* **2017**, *4* (6), 221−227.
(19) Liu, M.; Huang, X.; Song, Y.; Xu, T.; Wang, S.; Wu, Z.; Hu, M.; Zhang, L.; Zhang, Q.; Pan, Y.; Liu, X.; Zhu, T. Rapid SO_2 emission reductions significantly increase tropospheric ammonia concentrations over the North China Plain. *Atmos. Chem. Phys.* **2018**, *18* (24), 17933−17943.
(20) Nenes, A.; Pandis, S.; Weber, R.; Russell, A. Aerosol pH and liquid water content determine when particulate matter is sensitive to ammonia and nitrate availability. *Atmos. Chem. Phys.* **2020**, *20* (5), 3249−3258.
(21) Xu, Z.; Liu, M.; Zhang, M.; Song, Y.; Wang, S.; Zhang, L.; Xu, T.; Wang, T.; Yan, C.; Zhou, T.; Sun, Y.; Pan, Y.; Hu, M.; Zheng, M.; Zhu, T. High efficiency of livestock ammonia emission controls in alleviating particulate nitrate during a severe winter haze episode in northern China. *Atmos. Chem. Phys.* **2019**, *19* (8), 5605−5613.
(22) Huang, X.; Ding, A.; Gao, J.; Zheng, B.; Zhou, D.; Qi, X.; Tang, R.; Wang, J.; Ren, C.; Nie, W.; Chi, X.; Xu, Z.; Chen, L.; Li, Y.; Che, F.; Pang, N.; Wang, H.; Tong, D.; Qin, W.; Cheng, W.; Liu, W.; Fu, Q.; Liu, B.; Chai, F.; Davis, S.; Zhang, Q.; He, K. Enhanced secondary pollution offset reduction of primary emissions during COVID-19 lockdown in China. *Natl. Sci. Rev.* **2020**, *8* (2), nwaa137.
(23) Li, M.; Zhang, Z.; Yao, Q.; Wang, T.; Xie, M.; Li, S.; Zhuang, B.; Han, Y. Nonlinear responses of particulate nitrate to NO_x emission controls in the megalopolises of China. *Atmos. Chem. Phys.* **2021**, *21* (19), 15135−15152.
(24) Yang, S.; Yuan, B.; Peng, Y.; Huang, S.; Chen, W.; Hu, W.; Pei, C.; Zhou, J.; Parrish, D.; Wang, W.; He, X.; Cheng, C.; Li, X. B.; Yang, X.; Song, Y.; Wang, H.; Qi, J.; Wang, B.; Wang, C.; Wang, C.; Wang, Z.; Li, T.; Zheng, E.; Wang, S.; Wu, C.; Cai, M.; Ye, C.; Song, W.; Cheng, P.; Chen, D.; Wang, X.; Zhang, Z.; Wang, X.; Zheng, J.; Shao, M. The formation and mitigation of nitrate pollution: comparison between urban and suburban environments. *Atmos. Chem. Phys.* **2022**, *22* (7), 4539−4556.
(25) Wang, Y.; Zhao, Y.; Wang, Y.; Yu, J. Z.; Shao, J.; Liu, P.; Zhu, W.; Cheng, Z.; Li, Z.; Yan, N.; Xiao, H. Organosulfates in atmospheric aerosols in Shanghai, China: seasonal and interannual variability, origin, and formation mechanisms. *Atmos. Chem. Phys.* **2021**, *21* (4), 2959−2980.
(26) Zang, H.; Zhao, Y.; Huo, J.; Zhao, Q.; Fu, Q.; Duan, Y.; Shao, J.; Huang, C.; An, J.; Xue, L.; Li, Z.; Li, C.; Xiao, H. High atmospheric oxidation capacity drives wintertime nitrate pollution in the eastern Yangtze River Delta of China. *Atmos. Chem. Phys.* **2022**, *22* (7), 4355−4374.
(27) Zhang, Z.; Jiang, Z.; Guan, H.; Liang, Y.; Zheng, N.; Guo, W. Isotopic evidence for the high contribution of wintertime photochemistry to particulate nitrate formation in Northern China. *J. Geophys. Res.: Atmos.* **2021**, *126* (22), No. e2021JD035324.
(28) Zhao, D.; Liu, G.; Xin, J.; Quan, J.; Wang, Y.; Wang, X.; Dai, L.; Gao, W.; Tang, G.; Hu, B.; Ma, Y.; Wu, X.; Wang, L.; Liu, Z.; Wu, F. Haze pollution under a high atmospheric oxidization capacity in summer in Beijing: insights into formation mechanism of atmospheric physicochemical processes. *Atmos. Chem. Phys.* **2020**, *20* (8), 4575−4592.
(29) Li, K.; Jacob, D.; Liao, H.; Zhu, J.; Shah, V.; Shen, L.; Bates, K.; Zhang, Q.; Zhai, S. A two-pollutant strategy for improving ozone and particulate air quality in China. *Nat. Geosci.* **2019**, *12* (11), 906−910.
(30) Lu, K.; Fuchs, H.; Hofzumahaus, A.; Tan, Z.; Wang, H.; Zhang, L.; Schmitt, S. H.; Rohrer, F.; Bohn, B.; Broch, S.; Dong, H.; Gkatzelis, G. I.; Hohaus, T.; Holland, F.; Li, X.; Liu, Y.; Liu, Y.; Ma, X.; Novelli, A.; Schlag, P.; Shao, M.; Wu, Y.; Wu, Z.; Zeng, L.; Hu, M.; Kiendler-Scharr, A.; Wahner, A.; Zhang, Y. Fast photochemistry in wintertime haze: consequences for pollution mitigation strategies. *Environ. Sci. Technol.* **2019**, *53* (18), 10676−10684.
(31) Womack, C.; McDuffie, E.; Edwards, P.; Bares, R.; de Gouw, J.; Docherty, K.; Dubé, W. P.; Fibiger, D.; Franchin, A.; Gilman, J.; Goldberger, L.; Lee, B.; Lin, J.; Long, R.; Middlebrook, A.; Millet, D.; Moravek, A.; Murphy, J.; Quinn, P.; Riedel, T.; Roberts, J.; Thornton, J.; Valin, L.; Veres, P.; Whitehill, A.; Wild, R.; Warneke, C.; Yuan, B.; Baasandorj, M.; Brown, S. An odd oxygen framework for wintertime ammonium nitrate aerosol pollution in urban areas: NOx and VOC control as mitigation strategies. *Geophys. Res. Lett.* **2019**, *46* (9), 4971−4979.
(32) Xu, J.; Tie, X.; Gao, W.; Lin, Y.; Fu, Q. Measurement and model analyses of the ozone variation during 2006 to 2015 and its response to emission change in megacity Shanghai, China. *Atmos. Chem. Phys.* **2019**, *19* (14), 9017−9035.
(33) Ervens, B.; George, C.; Williams, J.; Buxton, G.; Salmon, G.; Bydder, M.; Wilkinson, F.; Dentener, F.; Mirabel, P.; Wolke, R.; Herrmann, H. CAPRAM 2.4 (MODAC mechanism): an extended and condensed tropospheric aqueous phase mechanism and its application. *J. Geophys. Res.: Atmos.* **2003**, *108* (D14), 4426.

https://doi.org/10.1021/acs.est.3c04629
Environ. Sci. Technol. 2023, 57, 15979−15989

(34) Stockwell, W.; Kirchner, F.; Kuhn, M.; Seefeld, S. A new mechanism for regional atmospheric chemistry modeling. *J. Geophys. Res.: Atmos.* **1997**, *102* (D22), 25847−25879.
(35) Xue, L.; Wang, T.; Guo, H.; Blake, D.; Tang, J.; Zhang, X.; Saunders, S.; Wang, W. Sources and photochemistry of volatile organic compounds in the remote atmosphere of western China: results from the Mt. Waliguan Observatory. *Atmos. Chem. Phys.* **2013**, *13* (17), 8551−8567.
(36) Zhang, Y.; Xue, L.; Carter, W.; Pei, C.; Chen, T.; Mu, J.; Wang, Y.; Zhang, Q.; Wang, W. Development of ozone reactivity scales for volatile organic compounds in a Chinese megacity. *Atmos. Chem. Phys.* **2021**, *21* (14), 11053−11068.
(37) Zhang, Y.; Xue, L.; Li, H.; Chen, T.; Mu, J.; Dong, C.; Sun, L.; Liu, H.; Zhao, Y.; Wu, D.; Wang, X.; Wang, W. Source apportionment of regional ozone pollution observed at Mount Tai, North China: application of Lagrangian photochemical trajectory model and implications for control policy. *J. Geophys. Res.: Atmos.* **2021**, *126* (6), No. e2020JD033519.
(38) Guo, H.; Sullivan, A.; Campuzano, P.; Schroder, J.; Lopez, F. D.; Dibb, J.; Jimenez, J.; Thornton, J.; Brown, S.; Nenes, A.; Weber, R. Fine particle pH and the partitioning of nitric acid during winter in the northeastern United States. *J. Geophys. Res.: Atmos.* **2016**, *121* (17), 10355−10376.
(39) Guo, H.; Xu, L.; Bougiatioti, A.; Cerully, K.; Capps, S.; Hite, J.; Carlton, A.; Lee, S.; Bergin, M.; Ng, N.; Nenes, A.; Weber, R. Fine-particle water and pH in the southeastern United States. *Atmos. Chem. Phys.* **2015**, *15* (9), 5211−5228.
(40) Li, M.; Zhang, Q.; Zheng, B.; Tong, D.; Lei, Y.; Liu, F.; Hong, C.; Kang, S.; Yan, L.; Zhang, Y.; Bo, Y.; Su, H.; Cheng, Y.; He, K. Persistent growth of anthropogenic non-methane volatile organic compound (NMVOC) emissions in China during 1990−2017: drivers, speciation and ozone formation potential. *Atmos. Chem. Phys.* **2019**, *19* (13), 8897−8913.
(41) Weng, H.; Lin, J.; Martin, R.; Millet, D. B.; Jaeglé, L.; Ridley, D.; Keller, C.; Li, C.; Du, M.; Meng, J. Global high-resolution emissions of soil NO_x, sea salt aerosols, and biogenic volatile organic compounds. *Sci. Data* **2020**, *7*, 148.
(42) Li, G.; Bei, N.; Cao, J.; Huang, R.; Wu, J.; Feng, T.; Wang, Y.; Liu, S.; Zhang, Q.; Tie, X.; Molina, L. T. A possible pathway for rapid growth of sulfate during haze days in China. *Atmos. Chem. Phys.* **2017**, *17* (5), 3301−3316.
(43) WHO. *WHO Global Air Quality Guidelines: Particulate Matter ($PM_{2.5}$ and PM_{10}), Ozone, Nitrogen Dioxide, Sulfur Dioxide and Carbon Monoxide*, 2021.
(44) Wang, H.; Wang, H.; Lu, X.; Lu, K.; Zhang, L.; Tham, Y. J.; Shi, Z.; Aikin, K.; Fan, S.; Brown, S. S.; Zhang, Y. Increased night-time oxidation over China despite widespread decrease across the globe. *Nat. Geosci.* **2023**, *16* (3), 217−223.

https://doi.org/10.1021/acs.est.3c04629
Environ. Sci. Technol. 2023, 57, 15979−15989